PERGAMON

International Journal of Heat and Mass Transfer 44 (2001) 1925–1936

International Journal of HEAT and MASS TRANSFER

www.elsevier.com/locate/ijhmt

Electron kinetic theory approach – one- and three-dimensional heating with pulsed laser

B.S. Yilbas *

Department of Mechanical Engineering, King Fahd University of Petroleum and Minerals, Dhahran 31261, Saudi Arabia

Received 19 October 1999; received in revised form 3 July 2000

Abstract

The modeling of laser heating process is essential for better understanding of the physical phenomena that occur as laser interacts with the workpiece. The Fourier heating model is not applicable for certain range of laser pulses. Consequently, new models of the laser heating process that eliminate this shortcoming of the Fourier heating model are needed. In the present study, a three-dimensional laser heating process based on the electron kinetic theory is introduced. The temperature profiles predicted from the kinetic theory are compared with the Fourier theory findings. The convergence of three-dimensional to one-dimensional heating is investigated. The electron kinetic theory predictions are also compared with the two-equation model results for a one-dimensional case. The study is extended to include two different laser pulse lengths. It is found that three-dimensional heating approaches its one-dimensional counterpart for the Gaussian intensity profile. As the pulse length shortens, the Fourier theory predicts higher temperatures in the surface region of the substrate as compared to that predicted from the electron kinetic theory. The temperature profiles obtained from the two-equation model and the kinetic theory are almost identical for the short pulse length employed in the present study.

1. Introduction

Lasers find wide application in various electronic industries because of their precision of operation, low cost, and resulting high quality of end product. The modeling of the heating process minimizes the experimental cost and gives insight into the physical phenomena involved during interaction between the laser and workpiece. Considerable research studies were conducted in the past to explore the laser heating process [1–3]. Most of these theoretical studies relied on the Fourier heating model, which did not give accurate results beyond certain ranges of laser pulses [4]. As the pulse length reduces to sub-nano-seconds, the Fourier heating model fails to predict the temperature profiles correctly [5]. This is because of the fact that the Fourier heating is only applicable when the spacing between two isothermal planes, where the heat conduction takes place, is greater than the interatomic spacing of the material. Harrington [6] showed that, in metals, electrons within a couple of electron mean free paths contribute over 98% of the total energy transported; in which case, the temperature gradient ($\partial\phi/\partial x$) should be constant over at least this distance. Consequently, the Fourier heating model should be applicable for distances not less than this distance. Moreover, in the Fourier heating model, high order temperature gradients ($\partial^3\phi/\partial x^3$, etc.) are omitted, but the high order terms play a significant role in short pulse laser heating. This is because the temperature gradient between two closely spaced planes is electron energy distribution dependent. Moreover, the depth of energy absorbed by the metal during laser radiation is almost on the order of a couple of mean free paths; therefore, at high laser power intensities and short interaction time, the temperature gradient across two closely spaced isothermal planes is not constant. In order to overcome the inaccuracy that arises in the Fourier heating model, a new model based on electron movement in the solid should be considered.

* Tel.: +966-03-860-4481; fax: +966-03-860-2949.
E-mail address: bsyilbas@dpc.kfupm.edu.sa (B.S. Yilbas).

0017-9310/01/$ - see front matter
PII: S0017-9310(00)00241-6

Nomenclature

A	area where electrons flux (m^2)
a	Gaussian parameter
C_{pe}	electron heat capacity (J/kg K)
C_{pl}	lattice heat capacity (J/kg K)
C_p	specific heat (J/kg K)
G	coupling factor (W/m^3 K)
$E(s,y,z,t)$	electron energy in the x-axis (J)
$E(x,\eta,z,t)$	electron energy in the y-axis (J)
$E(x,y,\zeta,t)$	electron energy in the z-axis (J)
$E(x,y,z,t)$	phonon energy (J)
f	fraction of excess energy exchange
h	Planck's constant (10^{-34} J s)
I_0	laser peak power intensity (W/m^2)
I_{surf}	laser power intensity at the surface (W/m^2)
k	thermal conductivity (W/m K)
k_B	Boltzmann's constant (1.38×10^{-23} J/K)
M	atomic mass (10^{-27} kg)
m_e	electron mass (10^{-31} kg)
N	electron number density ($1/m^3$)
r_f	reflection coefficient
S	source term
$\phi(x,y,z,t)$	lattice site temperature (K)
$\phi(x,t)$	phonon temperature in one-dimensional motion (K)
$\overline{V}$	electron mean velocity (m/s)
x,y,z	spatial coordinates in the x-, y-, z-axis for phonon (m)
s,η,ζ	spatial coordinates in the x-, y-, z-axis for electron movement (m)
$\delta(\omega)$	delta Dirac function
δ	absorption coefficient (1/m)
$\hbar$	Planck's constant (1.054592×10^{-34} Js)
$\theta(s,t)$	electron temperature in one-dimensional motion (K)
$\theta(s,y,z,t)$	electron temperature in the x-axis (K)
$\theta(x,\eta,z,t)$	electron temperature in the y-axis (K)
$\theta(x,y,\zeta,t)$	electron temperature in the z-axis (K)
λ	mean free path of electrons (m)
v	frequency (1/s)
ρ	density (kg/m^3)
τ	electron mean time between electron–phonon coupling (s)

Studies on non-equilibrium conduction heating were initiated earlier [7]. The existence of low specific heat of electrons allowed the consideration of the electrons being isolated from the lattice site for ultra-short duration of heating. In this case, the electron motion in surface vicinity under the electromagnetic radiation enabled the mechanisms of electron excitation and electron–phonon interactions to be considered when modeling the non-equilibrium heating process. The two-equation model was first introduced by Anisimov et al. [7] in this regard. In the later stage, the model was further investigated and the predictions were validated through the experimentation [8]. In the study, a picosecond laser pulse heating of copper was carried out and it was shown that the macroscopic calculations of energy relaxation in the two-equation system of electrons and phonons agreed with initial measurements of copper thermoreflectance transients at 100 and 300 K. Later, a two-equation model was introduced for short pulse heating of gold substrate by Qiu and Tien [9]. They indicated that the conventional one step radiation heating (Fourier heating model) over-predicted the heat-affected region. However, in a slow heating regime (nano second heating pulse), the two-equation model reduced to a Fourier heating model. The femtosecond laser heating of multi-layer metals was also studied by Qiu and Tien [10]. They showed that a multi-layer metallic system gave different responses to laser pulse heating as compared to a single-layer metal system. In this case, most of the absorbed energy was converted into lattice energy in the chromium layer rather than in the gold layer. The effect of interfacial roughness on phonon radiative heat conduction was examined by Majumder [11]. He indicated that due to the fractal characteristics of the surface, the amount of surface exposed to incident phonons increased with the frequency of phonons. Moreover, because of the increase in surface area, the resistance to heat transport by phonons decreased for higher frequencies. A unified approach for heat conduction from macro-to-micro scales was introduced by Tzou [12]. He proposed a universal equation between the heat flux vector and the temperature gradient to cover the fundamental behaviors of diffusion, wave, phonon–electron interactions, and pure phonon scattering. He indicated that the universal form of the energy equation facilitated the identification of physical parameters for transitions among the governing mechanisms. A relaxation model accounting for the finite velocity of heat propagation and the inertia of the internal heat source for the heat conduction and generation was introduced by Malinowski [13]. The finite velocity of heat propagation and the inertia of the internal heat source were considered in the hyperbolic heat conduction equation. He introduced the analytical solution of initial value problems for heat conduction and generation. He observed that unlike the classical hyperbolic model, the relaxation model did not tend to approach the corresponding parabolic solution.

Yilbas [14] introduced the electron kinetic theory approach pertinent to the laser pulse heating process.

The electron kinetic theory of heating relies on the electron lattice site atom collisions; in this case, the microscopic effects in the energy exchange mechanisms play a major role. The process of energy exchange mechanism can be described as follows: the energy gained by the electrons due to laser electromagnetic radiation is transferred to the lattice site atoms in the surface vicinity through successive electron lattice site atom collisions. This forces the neighboring atoms in the lattice to vibrate with higher amplitude resulting in increased lattice site temperature. The electron kinetic theory predictions for the temperature distribution in the surface vicinity of the substrate differ from the predictions of Fourier theory when the laser pulse length reduces to sub-nano-seconds [5]. The electron kinetic approach based on the collisional process was studied analytically for one-dimensional heating model [15]. The analysis was limited to one-dimensional heating case, which did not provide information on the temperature profiles in the radial direction due to pulse intensity distribution at the workpiece surface. Consequently, to examine the effect of pulse intensity distribution on the temperature profiles and to identify the deviation of temperature profiles due to sub-nano-second pulse laser heating, the present study is carried out. To predict the temperature profiles, the three-dimensional form of the electron kinetic theory approach is introduced and the differential form of the heat transfer equation is deduced using the Fourier transformation method as it was used in the previous study [15]. The predictions are compared with the Fourier heating model findings for the same pulse properties. The study is extended to include the comparison of the electron kinetic theory predictions with the two-equation model results.

2. Mathematical analysis and numerical solution

The three heat conduction models are presented under the appropriate sub-headings. In order to avoid lengthy arguments, only the necessary mathematical arrangements of the governing equations are given here. In the analysis, the laser power intensity profiles are assumed to be Gaussian and the spatial location of intensity distribution at $1/e$ points corresponds to $2/3$ of the laser beam diameter ($2r_0$, where r_0 is the laser beam radius 0.28×10^{-3} m). In this case, Gaussian intensity profile I_{surf} at the workpiece surface is

$$I_{\text{surf}}=\frac{I_0(1-r_f)}{\sqrt{\pi}a}\exp\left(-\frac{y^2+z^2}{a^2}\right),$$

where I_0 is the peak power intensity, r_f the surface reflectivity, and a is the Gaussian parameter.

2.1. Fourier heating model (one equation model)

The three-dimensional Fourier equation governing the laser heating pulse can be written as

$$\rho C_{\text{p}}\frac{\partial}{\partial t}\phi(x,y,z,t) = k\left(\frac{\partial^2\phi(x,y,z,t)}{\partial x^2}+\frac{\partial^2\phi(x,y,z,t)}{\partial y^2}+\frac{\partial^2\phi(x,y,z,t)}{\partial z^2}\right) + I_{\text{surf}}\delta\exp(-\delta x), \quad (1)$$

where I_{surf} is the pulse intensity distribution at the surface and δ is the absorption coefficient.

Since the heating takes place during a short duration of time and the size of the heated spot is considerably small, the convection and radiation losses from the surface are assumed to be negligible. In this case, the boundary condition at the surface yields ($x=0$)

$$\left.\frac{\partial\phi(x,y,z,t)}{\partial x}\right|_{x=0}=0$$

and the remaining boundary conditions are

$$\phi(\infty,y,z,t)=0:\phi(x,\infty,z,t)=0:\phi(x,y,\infty,t)=0.$$

The initial condition at $t=0$ is

$$\phi(x,y,z,0)=0.$$

The solution of Eq. (1) is obtained numerically with the appropriate boundary conditions.

2.2. Two-equation model

The non-equilibrium radiation heating process may be modeled through the two-step process [7]. These steps include: (i) the absorption of photon energy by electrons, and (ii) the heating of the lattice through electron–phonon coupling. The one-dimensional mathematical analysis of the model is given in the previous study [7]; therefore, only the governing equations in the one-dimensional form are presented herein. The equations representing the energy exchange mechanism during phonon absorption and electron–phonon coupling are

$$\frac{\partial\theta(s,t)}{\partial t}=\nabla(k\theta(s,t))-G[\theta(s,t)-\phi(x,t)]+S$$

and

$$C_{\text{l}}\frac{\partial\phi(x,t)}{\partial t}=G[\theta(s,t)-\phi(x,t)],$$

$\theta(s,t)$ and $\phi(x,t)$ are the electron and lattice site temperatures, S the laser source term ($I_0(1-r_f)\delta\exp(-\delta x)$), and C_{e} ($C_{\text{e}}=\rho C_{p\text{e}}$) and C_{l} ($C_{\text{l}}=\rho C_{p\text{l}}$) are the electron and lattice heat capacities, respectively. I_0 is the peak power intensity and G is the electron–phonon coupling factor, given by

$$G = \frac{\pi^2 m_e n_e \overline{V}^2}{6\tau\theta(s,t)},$$

where $m_e, n_e, \overline{V}, \tau, \theta(s,t)$ are electron mass, electron number density, electron mean velocity, the electron mean free time between electron–phonon coupling, and electron temperature, respectively. The governing equations are solved numerically.

2.3. Kinetic theory approach

Some parts of the analysis of the kinetic theory model dealing with the collision probabilities are not given here, but are referred to [14,15].

The absorption of the incident laser beam takes place in the x-axis; therefore, the intensity of the incident beam at any plane x inside the substrate is

$$I = I_{\text{surf}} \exp(-\delta x)$$

and in the limit, for a small section Δx resolved at x, the energy absorbed is

$$I = \delta I_{\text{surf}} \exp(-\delta x)$$

or

$$I = -I_{\text{surf}} \frac{\mathrm{d}}{\mathrm{d}x}[f(x)]$$

or

$$I = -I_{\text{surf}} f'(x),$$

where $f'(x)$ is the absorption function. The incident laser beam will be absorbed in a way described by

$$-f'(x) = \frac{\mathrm{d}}{\mathrm{d}x}[\exp(-\delta|x|)]$$

for all x.

Moreover, the possibility exists that electron number densities may vary throughout the material, i.e., the number of electrons traveling from ds to dx (Fig. 1) may not be the same as that from dx to ds. Consequently, the proportion of energy which is absorbed by electrons traveling from ds to dx in time dt is

$$-I_{\text{surf}} A_{yz}\, \mathrm{d}t\, \mathrm{d}\varphi f'(\varphi) \frac{N_{sx}}{N_{sx} + N_{xs}},$$

where A_{yz} is the area that electrons pass through in the x-axis, $f'(\varphi)$ the absorption function $(\mathrm{d}/\mathrm{d}\varphi[\exp(-\delta|\varphi|)])$, N_{sx} and N_{xs} are the number of electrons traveling from bulk to surface (s to x) and surface to bulk (x to s) as depicted in Fig. 1. Therefore, the total amount of energy absorbed by the electrons from dx to ds is

$$\Delta E_{\text{Absorption}} = \int_0^x I_{\text{surf}} \frac{f'(\varphi) N_{sx}}{(N_{sx} + N_{xs})\overline{V}}\, \mathrm{d}\varphi,$$

where $\overline{V}$ is the mean velocity of the electrons.

The amount of energy which electrons transfer to the lattice site atoms in the surface vicinity can be formulated as follows.

The amount of energy which electrons transfer to the lattice site atoms in the x-axis can be written as [14,15]

$$\Delta E_x = \mathrm{d}x\, \mathrm{d}t A_{yz} \int_{-\infty}^{\infty} \frac{N_{sx}\overline{V} f k_B}{\lambda^2} \times \exp\left(-\frac{|x-s|}{\lambda}\right)[\theta(s,y,z,t) - \phi(x,y,z)]\, \mathrm{d}s,$$

where A_{yz} is the area that electrons pass over in the x-axis ($A_{yz} = \mathrm{d}y\, \mathrm{d}z$) and λ is the mean free path.

The total amount of energy which transfers to the lattice site atoms due to successive electrons lattice site atoms collisions in the y- and z-axes can be written similarly to that written for the x-axis. The total amount of energy transfer to lattice site atoms in the y-axis is

$$\Delta E_y = A_{xz}\, \mathrm{d}y\, \mathrm{d}t \int_{-\infty}^{\infty} \frac{N_{\eta y}\overline{V} f k_B}{\lambda^2} \times \exp\left(-\frac{|y-\eta|}{\lambda}\right)[\theta(x,\eta,z,t) - \phi(x,y,z)]\, \mathrm{d}\eta.$$

Total amount of energy transfer to lattice site atoms in the z-axis is

$$\Delta E_z = A_{xy}\, \mathrm{d}z\, \mathrm{d}t \int_{-\infty}^{\infty} \frac{N_{\varsigma z}\overline{V} f k_B}{\lambda^2} \times \exp\left(-\frac{|y-\varsigma|}{\lambda}\right)[\theta(x,y,\varsigma,t) - \phi(x,y,z)]\, \mathrm{d}\varsigma,$$

where A_{xz} is the area that electrons pass over in the y-axis ($A_{xz} = \mathrm{d}x\, \mathrm{d}z$) and A_{xy} is the area that electrons cross over in the z-axis ($A_{xy} = \mathrm{d}x\, \mathrm{d}y$).

The total amount of energy transfer to the lattice site atoms in the x-, y-, and z-axes due to the collisional process is

$$\Delta E = \Delta E_x + \Delta E_y + \Delta E_z$$

or the total amount of energy transfer per unit volume and per unit time dt is:

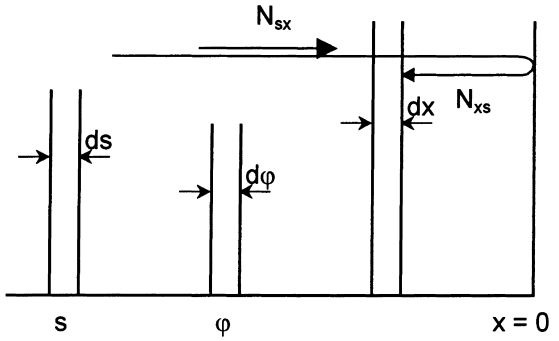

Fig. 1. Electron movement in the surface vicinity ($x = 0$ is the surface).

$$\frac{\Delta E}{\mathrm{d}x\,\mathrm{d}y\,\mathrm{d}z\,\mathrm{d}t} = \int_{-\infty}^{\infty} \frac{N_{sx}\overline{V}fk_{\mathrm{B}}}{\lambda^2} \exp\left(-\frac{|x-s|}{\lambda}\right)[\theta(s,y,z,t) - \phi(x,y,z)]\,\mathrm{d}s + \int_{-\infty}^{\infty} \frac{N_{\eta y}\overline{V}fk_{\mathrm{B}}}{\lambda^2} \times \exp\left(-\frac{|y-\eta|}{\lambda}\right)[\theta(x,\eta,z,t) - \phi(x,y,z)]\,\mathrm{d}\eta + \int_{-\infty}^{\infty} \frac{N_{\varsigma z}\overline{V}fk_{\mathrm{B}}}{\lambda^2} \times \exp\left(-\frac{|y-\varsigma|}{\lambda}\right)[\theta(x,y,\varsigma,t) - \phi(x,y,z)]\,\mathrm{d}\varsigma.$$

Since the energy which is transferred to the lattice site atoms in the collisional process results in a change of both potential and vibration energy, then

$$\frac{\Delta E}{\mathrm{d}x\,\mathrm{d}y\,\mathrm{d}z\,\mathrm{d}t} + \Delta E_{\mathrm{Absorption}} = \frac{\partial}{\partial t}[NM(U_0 + 3k_{\mathrm{B}}\phi(x,t))] = \rho C_{\mathrm{p}}\frac{\partial\phi(x,y,z,t)}{\partial t} \tag{2}$$

and the complete energy equation for the collisional process becomes

$$\rho C_{\mathrm{p}}\frac{\partial\phi(x,y,z,t)}{\partial t} = \int_{-\infty}^{\infty} \frac{N_{sx}\overline{V}fk_{\mathrm{B}}}{\lambda^2} \times \exp\left(-\frac{|x-s|}{\lambda}\right)[\theta(s,y,z,t) - \phi(x,y,z)]\,\mathrm{d}s + \int_{-\infty}^{\infty} \frac{N_{\eta y}\overline{V}fk_{\mathrm{B}}}{\lambda^2} \exp\left(-\frac{|y-\eta|}{\lambda}\right)[\theta(x,\eta,z,t) - \phi(x,y,z)]\,\mathrm{d}\eta + \int_{-\infty}^{\infty} \frac{N_{\varsigma z}\overline{V}fk_{\mathrm{B}}}{\lambda^2} \times \exp\left(-\frac{|y-\varsigma|}{\lambda}\right)[\theta(x,y,\varsigma,t) - \phi(x,y,z)]\,\mathrm{d}\varsigma + \int_{-\infty}^{\infty} \frac{I_{\mathrm{surf}}}{\lambda^2}\frac{fN_{sx}}{N_{sx}+N_{xs}} \exp\left(-\frac{|x-s|}{\lambda}\right)\int_x^s f'(\varphi)\,\mathrm{d}\varphi\,\mathrm{d}s. \tag{3}$$

The final temperature of the electrons in the volume element ($\mathrm{d}x\ \mathrm{d}y\,\mathrm{d}z$) after the collisional process can be readily found from the conservation of energy, i.e.

Total electron energy after collision

= Total electron energy during $\mathrm{d}t$

− Change of lattice site energy

The total electron energy after collision is as follows:

$$\int_{-\infty}^{\infty} \frac{N_{sx}\overline{V}(1-f)k_{\mathrm{B}}}{\lambda^2} \exp\left(-\frac{|x-s|}{\lambda}\right)\theta(s,y,z,t)\,\mathrm{d}s,$$
$$\int_{-\infty}^{\infty} \frac{N_{\eta y}\overline{V}(1-f)k_{\mathrm{B}}}{\lambda^2} \exp\left(-\frac{|x-\eta|}{\lambda}\right)\theta(x,\eta,z,t)\,\mathrm{d}\eta,$$
$$\int_{-\infty}^{\infty} \frac{N_{\varsigma z}\overline{V}(1-f)k_{\mathrm{B}}}{\lambda^2} \exp\left(-\frac{|x-\varsigma|}{\lambda}\right)\theta(x,y,\varsigma,t)\,\mathrm{d}\varsigma. \tag{4}$$

The total electron energy carried into volume element during $\mathrm{d}t$ is

$$\int_{-\infty}^{\infty} \frac{N_{sx}\overline{V}k_{\mathrm{B}}}{\lambda^2} \exp\left(-\frac{|x-s|}{\lambda}\right)\theta(s,y,z,t)\,\mathrm{d}s + \int_{-\infty}^{\infty} \frac{N_{\eta y}\overline{V}k_{\mathrm{B}}}{\lambda^2} \exp\left(-\frac{|x-\eta|}{\lambda}\right)\theta(x,\eta,z,t)\,\mathrm{d}\eta + \int_{-\infty}^{\infty} \frac{N_{\varsigma z}\overline{V}k_{\mathrm{B}}}{\lambda^2} \exp\left(-\frac{|x-\varsigma|}{\lambda}\right)\theta(x,y,\varsigma,t)\,\mathrm{d}\varsigma + \int_{-\infty}^{\infty} \frac{I_0 f}{\lambda^2}\frac{N_{sx}}{N_{sx}+N_{xs}} \exp\left(-\frac{|x-s|}{\lambda}\right)\int_x^s f'(\varphi)\,\mathrm{d}\varphi\,\mathrm{d}s \tag{5}$$

and the change of lattice site atom energy is

$$\rho C_{\mathrm{p}}\frac{\partial\phi(x,y,z,t)}{\partial t}$$

as given by Eq. (2).

Consequently, substituting Eqs. (2), (4), and (5) into the requirement of the conservation of energy gives

$$\int_{-\infty}^{\infty} \frac{N_{sx}\overline{V}k_{\mathrm{B}}}{\lambda^2} \exp\left(-\frac{|x-s|}{\lambda}\right)[\theta(s,y,z,t) - f\phi(x,y,z,t)]\,\mathrm{d}s + \int_{-\infty}^{\infty} \frac{N_{\eta y}\overline{V}k_{\mathrm{B}}}{\lambda^2} \times \exp\left(-\frac{|x-\eta|}{\lambda}\right)[\theta(x,\eta,z,t) - f\phi(x,y,z,t)]\,\mathrm{d}\eta + \int_{-\infty}^{\infty} \frac{N_{\varsigma z}\overline{V}k_{\mathrm{B}}}{\lambda^2} \exp\left(-\frac{|x-\varsigma|}{\lambda}\right)[\theta(x,y,\varsigma,t) - f\phi(x,y,z,t)]\,\mathrm{d}\varsigma = \int_{-\infty}^{\infty} \frac{N_{sx}\overline{V}k_{\mathrm{B}}}{\lambda^2} \exp\left(-\frac{|x-s|}{\lambda}\right)(1-f)\theta(s,y,z,t)\,\mathrm{d}s + \int_{-\infty}^{\infty} \frac{N_{\eta y}\overline{V}k_{\mathrm{B}}}{\lambda^2} \exp\left(-\frac{|x-\eta|}{\lambda}\right)(1-f)\theta(x,\eta,z,t)\,\mathrm{d}\eta + \int_{-\infty}^{\infty} \frac{N_{\varsigma z}\overline{V}k_{\mathrm{B}}}{\lambda^2} \exp\left(-\frac{|x-\varsigma|}{\lambda}\right)(1-f)\theta(x,y,\varsigma,t)\,\mathrm{d}\varsigma + \int_{-\infty}^{\infty} (1-f)\frac{N_{sx}}{N_{sx}+N_{xs}} \times \exp\left(-\frac{|x-s|}{\lambda}\right)\int_x^s f'(\varphi)\,\mathrm{d}\varphi\,\mathrm{d}s. \tag{6}$$

Eqs. (3) and (6) have been kept in general form; however, it may be useful to consider a particular case, where electrons cannot escape through the surface (which may equally apply when a steady state space charge exists [14]).

In this case, the assumption that all directions of travel are equally probable gives

$$N_{sx} = N_{xs} = \frac{N}{6}, \tag{7}$$

where N is the number of free electrons per unit volume. In this case, Eqs. (5) and (8) yield

$$\rho C_{\mathrm{p}}\frac{\partial\phi(x,y,z,t)}{\partial t} = \int_{-\infty}^{\infty}\frac{fk}{\lambda^3}\exp\left(-\frac{|x-s|}{\lambda}\right)[\theta(s,y,z,t)-\phi(x,y,z)]\,\mathrm{d}s + \int_{-\infty}^{\infty}\frac{fk}{\lambda^3}\exp\left(-\frac{|y-\eta|}{\lambda}\right)[\theta(x,\eta,z,t)-\phi(x,y,z)]\,\mathrm{d}\eta + \int_{-\infty}^{\infty}\frac{fk}{\lambda^3}\exp\left(-\frac{|y-\varsigma|}{\lambda}\right)[\theta(x,y,\varsigma,t)-\phi(x,y,z)]\,\mathrm{d}\varsigma + \int_{-\infty}^{\infty}\frac{I_{\mathrm{surf}}}{\lambda^2}\frac{fN_{sx}}{N_{sx}+N_{xs}}\exp\left(-\frac{|x-s|}{\lambda}\right)\int_{x}^{s}f'(\varphi)\,\mathrm{d}\varphi\,\mathrm{d}s \tag{8}$$

which makes use of the simple kinetic theory result for the thermal conductivity

$$k=\frac{N\overline{V}k_{\mathrm{B}}\lambda}{6}$$

and

$$\int_{-\infty}^{\infty}\frac{k}{\lambda^3}\exp\left(-\frac{|x-s|}{\lambda}\right)[\theta(s,y,z,t)-f\phi(x,y,z,t)]\,\mathrm{d}s + \int_{-\infty}^{\infty}\frac{k}{\lambda^3}\exp\left(-\frac{|x-\eta|}{\lambda}\right)[\theta(x,\eta,z,t)-f\phi(x,y,z,t)]\,\mathrm{d}\eta + \int_{-\infty}^{\infty}\frac{k}{\lambda^3}\exp\left(-\frac{|x-\varsigma|}{\lambda}\right)[\theta(x,y,\varsigma,t)-f\phi(x,y,z,t)]\,\mathrm{d}\varsigma = \int_{-\infty}^{\infty}\frac{k}{\lambda^3}\exp\left(-\frac{|x-s|}{\lambda}\right)(1-f)\theta(s,y,z,t)\,\mathrm{d}s + \int_{-\infty}^{\infty}\frac{k}{\lambda^3}\exp\left(-\frac{|x-\eta|}{\lambda}\right)(1-f)\theta(x,\eta,z,t)\,\mathrm{d}\eta + \int_{-\infty}^{\infty}\frac{k}{\lambda^3}\exp\left(-\frac{|x-\varsigma|}{\lambda}\right)(1-f)\theta(x,y,\varsigma,t)\,\mathrm{d}\varsigma + \int_{-\infty}^{\infty}(1-f)\frac{N_{sx}}{N_{sx}+N_{xs}}\exp\left(-\frac{|x-s|}{\lambda}\right)\int_{x}^{s}f'(\varphi)\,\mathrm{d}\varphi\,\mathrm{d}s. \tag{9}$$

Eqs. (8) and (9) are the equations of interest for laser machining. The method of solution to be used in the following analysis is the transformation of the simultaneous differential–integral Eqs. (8) and (9) using the Fourier integral transformation, with respect to x, y, and z. The resultant ordinary differential equations may then be handled much more conveniently. Although, three-dimensional analysis of Fourier transformation, which is considered in the present study, is similar to that carried out for one-dimensional model studied previously [15], some of the details of these transformations are also presented below. This enhances the understanding of each step involved in the Fourier transformation for three-dimensional case.

Consider first reduction of the set of equations to the differential equation of heat conduction. The Fourier transformation of a function $f(x)$ is defined by

$$F[f(x)]=\int_{-\infty}^{\infty}\exp(-\mathrm{i}\omega x)f(x)\,\mathrm{d}x=F(\omega)$$

and the Fourier inversion by

$$f(x)=\frac{1}{2\pi}\int_{-\infty}^{\infty}F(\omega)(\exp(-\mathrm{i}\omega x)\,\mathrm{d}\omega.$$

The Fourier transformation of the convolution integral

$$\int_{-\infty}^{\infty}f(\xi)g(x-s)\,\mathrm{d}s$$

is the product of the transforms

$$\overline{f}(\omega)\cdot\overline{g}(\omega)$$

and the transform of function $\exp(-|x|/\lambda)$ is

$$\frac{2\lambda}{1+\omega^2\lambda^2}.$$

The Fourier transform of the function

$$\Phi=\int_{-\infty}^{\infty}\frac{k}{\lambda^3}\exp\left(-\frac{|x-s|}{\lambda}\right)\phi(x,t)\,\mathrm{d}s$$

will be a constant factor (the value of integral) multiplying the transform of the function $\phi(x,t)$, i.e.,

$$F[\Phi]=\frac{kf}{\lambda^3}\overline{\phi}F\left\{\int_{-\infty}^{\infty}\exp\left(-\frac{|x-s|}{\lambda}\right)\mathrm{d}s\right\}$$

or

$$F[\Phi]=\frac{kf}{\lambda^3}\overline{\phi}F\left\{\int_{-\infty}^{\infty}\exp\left(-\frac{|x-s|}{\lambda}\right)H(|s|)\,\mathrm{d}s\right\},$$

where $H(|s|)=1$ for $-\infty<s<\infty$.

Therefore:

$$F[\Phi]=\frac{kf}{\lambda^3}\overline{\phi}F\left\{\int_{-\infty}^{\infty}\exp\left(-\frac{|x-s|}{\lambda}\right)\right\}F\{H(|s|)\,\mathrm{d}s\} \leqslant \frac{kf}{\lambda^3}\overline{\phi}\frac{2\lambda}{\omega_x^2\lambda^2+1}\delta(\omega_x),$$

where $\delta(\omega_x)$ is the Dirac delta function. Since this function only has a value of 1 at $\omega_x=0$, then the transform is

$$\frac{kf}{\lambda^2}\overline{\phi}$$

These results can also be applicable for the y- and z-axes. Consequently, using these results, Eqs. (8) and (9) can be Fourier transformed, the result of which is:

$$\overline{\frac{\partial}{\partial t}(\rho C_{\mathrm{p}}\phi)} = \frac{kf}{\lambda^3}\left[\frac{2\lambda}{\omega_x^2\lambda^2+1}\overline{\theta}\right]+\frac{kf}{\lambda^3}\left[\frac{2\lambda}{\omega_y^2\lambda^2+1}\overline{\theta}\right] \times\frac{kf}{\lambda^3}\left[\frac{2\lambda}{\omega_z^2\lambda^2+1}\overline{\theta}\right]-\frac{kf}{\lambda^2}\overline{\phi} + \left[\frac{I_0\delta f}{2\lambda}\right]\left[\frac{2\lambda}{\omega_x^2\lambda^2+1}\right]\left[\frac{2\delta}{\delta^2+\omega_x^2}\right] \tag{10}$$

and

$$\frac{k}{\lambda^2}\left[\overline{\theta}-f\overline{\phi}\right]=\left[\frac{k(1-f)}{\lambda^3}\right]\left[\frac{2\lambda}{\omega_x^2\lambda^2+1}\right]\overline{\theta}+\left[\frac{k(1-f)}{\lambda^3}\right]\left[\frac{2\lambda}{\omega_y^2\lambda^2+1}\right]\overline{\theta}+\left[\frac{k(1-f)}{\lambda^3}\right]\left[\frac{2\lambda}{\omega_z^2\lambda^2+1}\right]\overline{\theta}+\frac{I_0\delta(1-f)}{2\lambda}\left[\frac{2\lambda}{\omega_x^2\lambda^2+1}\right]\left[\frac{2\delta}{\delta^2+\omega_x^2}\right]. \tag{11}$$

If the transform function $\overline{\theta}$ is eliminated from Eqs. (10) and (11), the result is

$$\left[f+(\omega_x^2+\omega_y^2+\omega_z^2)\lambda^2\right]\rho C_{\mathrm{p}}\overline{\frac{\partial}{\partial t}(\phi)}=-(\omega_x^2+\omega_y^2+\omega_z^2)kf\overline{\phi}+I_{\mathrm{surf}}\delta f\left[\frac{2\delta}{\delta^2+\omega_x^2}\right].$$

The multiplication in the transform domain by $(\mathrm{i}\omega_{x,y,z})^2$ corresponds to second order differential in the real plane. Hence, the inversion of the above equation gives

$$\left[f-\lambda^2\left(\frac{\partial^2}{\partial x^2}+\frac{\partial^2}{\partial y^2}+\frac{\partial^2}{\partial z^2}\right)\right]\rho C_{\mathrm{p}}\frac{\partial\phi}{\partial t}=kf\left(\frac{\partial^2\phi}{\mathrm{d}x^2}+\frac{\partial^2\phi}{\mathrm{d}y^2}+\frac{\partial^2\phi}{\mathrm{d}z^2}\right)+I_{\mathrm{surf}}\delta f\exp(-\delta|x|). \tag{12}$$

Dividing Eq. (12) by f and rearranging yields

$$\left[1-\frac{\lambda^2}{f}\left(\frac{\partial^2}{\partial x^2}+\frac{\partial^2}{\partial y^2}+\frac{\partial^2}{\partial z^2}\right)\right]\rho C_{\mathrm{p}}\frac{\partial\phi}{\partial t}=k\left(\frac{\partial^2\phi}{\mathrm{d}x^2}+\frac{\partial^2\phi}{\mathrm{d}y^2}+\frac{\partial^2\phi}{\mathrm{d}z^2}\right)+I_{\mathrm{surf}}\delta\exp(-\delta|x|). \tag{13}$$

The lattice site temperature can be obtained from Eq. (13), which is the differential form of Eqs. (8) and (9). Three-dimensional form of the energy equation is different than its counterpart that obtained for one-dimensional case, i.e., an additional term $[\lambda^2/f(\partial^2/\partial y^2+\partial^2/\partial z^2)]\rho C_{\mathrm{p}}\partial\phi/\partial t]$ representing the non-equilibrium heating in the y- and z-axes appears in three-dimensional form of the governing equation. Moreover, if the term $\lambda^2/f(\partial^2/\partial x^2+\partial^2/\partial x^2+\partial^2/\partial x^2)(\rho C_{\mathrm{p}}\partial\phi/\partial t)$ is neglected for all f values, Eq. (13) becomes

$$\rho C_{\mathrm{p}}\frac{\partial\phi}{\partial t}=k\left(\frac{\partial^2\phi}{\mathrm{d}x^2}+\frac{\partial^2\phi}{\mathrm{d}x^2}+\frac{\partial^2\phi}{\mathrm{d}x^2}\right)+I_{\mathrm{surf}}\delta\exp(-\delta|x|)$$

which is exactly the same as a Fourier heat conduction Eq. (3). The equations derived from the electron kinetic theory approach for the heat conduction process are more general than the Fourier equation.

2.4. Numerical solution

The numerical method employed uses a finite difference scheme, which is well established in the literature [16]. In order to obtain accurate results, the convergency criteria should be met. The stability criteria for each model are given as follows:

One-equation model:

$$1\geqslant ABS\left\{\frac{\rho C_{\mathrm{p}}}{\Delta t}-2k\left[\frac{1}{(\Delta x)^2}+\frac{1}{(\Delta y)^2}+\frac{1}{(\Delta z)^2}\right]\right\}+ABS\left\{\frac{k}{(\Delta x)^2}+\frac{k}{(\Delta y)^2}+\frac{k}{(\Delta z)^2}\right\}-ABS\left\{\frac{\rho C_{\mathrm{p}}}{\Delta t}\right\}$$

Two-equation model:

$$ABS\left|1-\frac{2k\Delta t}{\rho C_{\mathrm{p}}(\Delta x)^2}-\frac{G\Delta t}{\rho C_{\mathrm{p}}}\right|+ABS\left|\frac{2k\Delta t}{\rho C_{\mathrm{p}}(\Delta x)^2}\right|<1$$

Electron kinetic theory approach:

$$1\geqslant ABS\left[\frac{f\rho C_{\mathrm{p}}}{\Delta t}+2\lambda^2\rho C_{\mathrm{p}}\left[\frac{1}{\Delta t(\Delta x)^2}+\frac{1}{\Delta t(\Delta y)^2}+\frac{1}{\Delta t(\Delta z)^2}\right]-2kf\left[\frac{1}{(\Delta x)^2}+\frac{1}{(\Delta y)^2}+\frac{1}{(\Delta z)^2}\right]\right]+ABS\left\{\frac{kf}{(\Delta x)^2}-\frac{2\lambda^2\rho C_{\mathrm{p}}}{\Delta t(\Delta x)^2}\right\}+ABS\left\{\frac{kf}{(\Delta y)^2}-\frac{2\lambda^2\rho C_{\mathrm{p}}}{\Delta t(\Delta y)^2}\right\}+ABS\left\{\frac{kf}{(\Delta z)^2}-\frac{2\lambda^2\rho C_{\mathrm{p}}}{\Delta t(\Delta z)^2}\right\}+ABS\left\{\frac{2\lambda^2\rho C_{\mathrm{p}}}{\Delta t(\Delta x)^2}+\frac{2\lambda^2\rho C_{\mathrm{p}}}{\Delta t(\Delta y)^2}+\frac{2\lambda^2\rho C_{\mathrm{p}}}{\Delta t(\Delta z)^2}\right\}-ABS\left\{\frac{f\rho C_{\mathrm{p}}}{\Delta t}+2\lambda^2\rho C_{\mathrm{p}}\left[\frac{1}{\Delta t(\Delta x)^2}+\frac{1}{\Delta t(\Delta y)^2}+\frac{1}{\Delta t(\Delta z)^2}\right]\right\}$$

where Δx, Δy, and Δz are spatial increments in x-, y-, and z-axes while Δt is the time increment.

Gold is used as the workpiece material. The selection of gold is because of its thermo-physical properties, which are available in the literature [9]. The thermo-

Table 1
Thermal properties of gold used in the computation (9)

δ (1/m)	α (m^2/s)	C_{l} (J/m^3 K)	k (W/m K)	G (W/m^3 K)	C_{e} (W/m^3 K)
6.16×10^7	1.26×10^{-4}	2.5×10^6	315	2.6×10^{16}	2.1×10^4

Table 2
Power intensity, pulse length, and f value used in the computation

Power intensity $I_0(1-r_f)$ (W/m^2)	0.5×10^{11}	0.5×10^{11}
Pulse length (s)	6×10^{-11}	6×10^{-10}
f	1×10^{-4}	0.6×10^{-4}

physical properties of gold are given in Table 1 while the pulse properties are given in Table 2.

3. Results and discussion

The comparison of predictions from the Fourier heating, two-equation model, and electron kinetic theory approach is made for the one-dimensional heating case while the findings from the one and three-dimensional models of Fourier heating and electron kinetic theory approach are presented later herein. A gold substrate is used for one-dimensional heating and the pulse intensity is kept as the same for all models in the computation.

3.1. Comparison of the Fourier, two-equation and electron kinetic theory model predictions

The temperature profiles predicted from the Fourier theory, two-equation model, and kinetic theory approach are shown in Figs. 2 and 3 for two pulse lengths. All the temperature profiles become almost identical for a long pulse length. In this case, the two-equation and electron kinetic theory predictions approach the predictions of the Fourier heating model. Small discrepancies at the upper end of the temperature profiles are negligibly small. As the pulse length reduces to 6×10^{-11} s, the heating time also reduces. The temperature profiles predicted from all models differ considerably

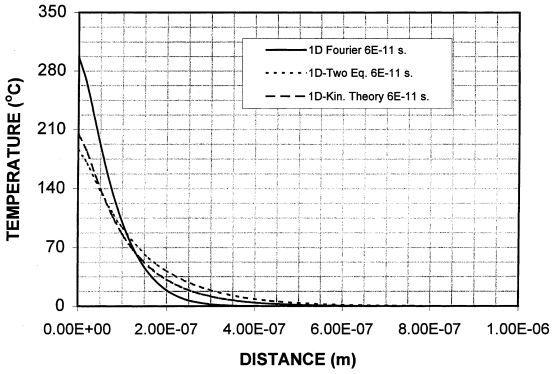

Fig. 2. Comparison of Fourier, two-equation and electron kinetic theory predictions for $6E\times10^{-11}$ s pulse length, and at $y=0$ and $z=0$.

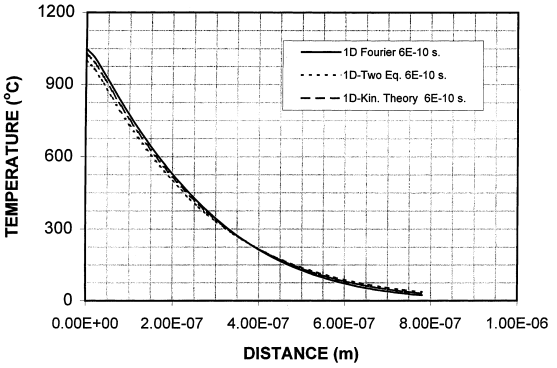

Fig. 3. Comparison of Fourier, two-equation and electron kinetic theory predictions for $6E\times10^{-10}$ s pulse length, and at $y=0$ and $z=0$.

provided that the two-equation model predicts similar temperature profiles to that predicted from the electron kinetic theory. The difference in temperature profiles occurs because of the fact that the electrons in the surface vicinity absorb the incident laser energy and the excited electrons do not make sufficient collisions with the lattice site atoms to transfer their excess energy in the surface region. Consequently, lattice site temperature in this region becomes lower than the electron temperature as evident from Fig. 4 in which the electron temperature distribution inside the substrate is shown. Therefore, the Fourier theory fails to predict the temperature rise in the surface vicinity accurately for a heating time of 6×10^{-11} s. On the other hand, small discrepancies occur between the electron kinetic theory and two-equation model predictions. This is due to one or all of the following facts: (i) the f value (fraction of excess electron energy transferred to the lattice site) is kept constant during the computations, which may be electron energy dependent, and (ii) the coupling factor in the two-equation model is assumed constant in the analysis; however, the coupling factor is electron mean velocity and temperature dependent. Consequently, this as-

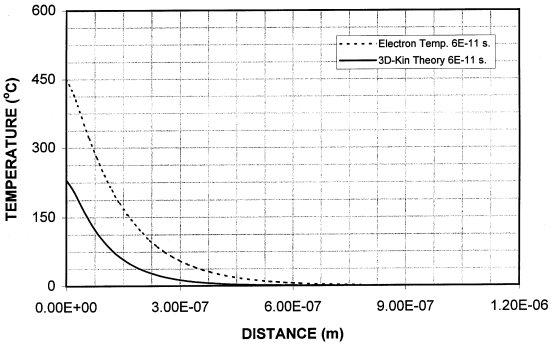

Fig. 4. Electron and lattice site temperatures for short pulse length, and at $y=0$ and $z=0$.

sumption may result in low temperature rise in the surface vicinity at early heating times.

3.2. Predictions of three- and one-dimensional heating

Fig. 5(a) shows the temperature profiles inside the substrate predicted from the three-dimensional and one-dimensional models of Fourier theory while Fig. 5(b) shows the temperature profiles inside the substrate predicted from the three-dimensional and one-dimensional models of electron kinetic theory for two pulse lengths. The temperature profiles are obtained at $y = 0$ and $z = 0$. The temperature profiles predicted from three- and one-dimensional cases are identical for both pulse lengths. This occurs because (i) the radial conduction in the central region of the heated spot is not considerable, which in turn results in one-dimensional conduction heating, and (ii) power intensity distribution is Gaussian and the power intensity is maximum at the beam center. This leads to considerable energy input supplied at the center of the heated solid; therefore, heating approaches one-dimensional behavior. This may also indicate that the collisional process yields to one-dimensional behavior and the heat transfer in radial direction due to the collisional process is not substantial. Similar arguments are also true for the Fourier heating case.

Figs. 6(a) and (b) show the comparative temperature profiles obtained from the Fourier and electron kinetic theory models for two pulse lengths. The temperature profiles predicted from electron kinetic theory model for short pulse length (6×10^{-11} s) give lower temperature in the vicinity of the surface as compared to the Fourier theory results. As the distance from the surface increases further inside the substrate the temperature profiles that result from the kinetic theory attain higher values as compared to the Fourier theory predictions. This indicates that the collisional energy transfer to the lattice site is not substantial at the short heating time, 6×10^{-11} s. In this case, the energy absorbed by the electrons does not make enough collisions with the lattice site atoms in the surface vicinity. The electrons, therefore, transfer their excess energy to lattice site atoms in the region next to the surface vicinity through the collisional process. As the heating pulse length increases, the predictions of electron kinetic theory converge to the Fourier theory predictions. This occurs because of the Fourier heating

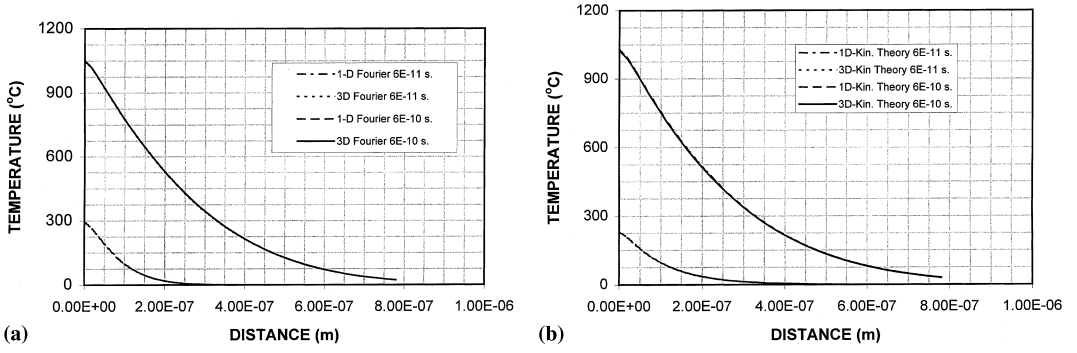

Fig. 5. (a) One- and three-dimensional Fourier theory results for pulse lengths of $6E \times 10^{-11}$ and $6E \times 10^{-10}$ s, and at $y = 0$ and $z = 0$; (b) one- and three-dimensional kinetic theory results for pulse lengths of $6E \times 10^{11}$ s and $6E \times 10^{10}$ s, and at $y = 0$ and $z = 0$.

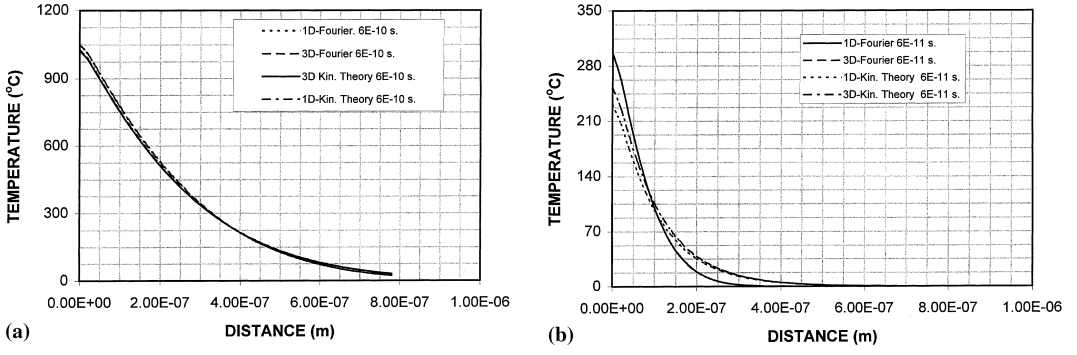

Fig. 6. (a) Temperature profiles predicted from the Fourier and kinetic theory in the x-axis for a pulse length of $6E \times 10^{-10}$ s, and at $y = 0$ and $z = 0$; (b) temperature profiles predicted from the Fourier and kinetic theory in the x-axis for a pulse length of $6E \times 10^{-11}$ s, and at $y = 0$ and $z = 0$.

dominates the conduction process; in which case, the term $(\partial/\partial t)(\partial^2\phi/\partial x^2)$ in the kinetic theory model (Eq. (13)) has no significant effect on the resulting temperature distributions. The electrons make considerable collisions with the lattice site atoms in the surface vicinity resulting in increased lattice site temperature for long pulse length (6×10^{-10} s). The temperature difference in the surface vicinity and the region next to surface vicinity enhances the phonon relaxation process, i.e., the conduction heat transfer into solid substrate substantiates.

Fig. 7 shows the temperature gradient $(\partial\phi/\partial x)$ predicted from the Fourier and electron kinetic theories with the distance in the x-axis for two pulse lengths. The temperature gradients predicted from both theories are similar for the long pulse length (6×10^{-10} s). In general, the temperature gradient decreases sharply in the surface vicinity to reach its minimum. As the distance from the point of minimum increases further inside the substrate, $\partial\phi/\partial x$ increases gradually. The sharp decrease of $\partial\phi/\partial x$ in the surface vicinity is due to the rapid increase of the temperature in this region. In this case, the energy absorbed by the electrons in the surface vicinity is converted into the internal energy gain of the substrate through collisional process. This gives rise to a sharp rise of the lattice site temperature. The energy balance attains among the absorbed energy, internal energy gain, and the conduction process at the point of minimum $\partial\phi/\partial x$ [17]. As the distance increases beyond the point of minimum, the gradual increase in $\partial\phi/\partial x$ reveals that the conduction effect due to phonon relaxation dominates. However, as the pulse length reduces, the temperature gradients predicted from both theories differ considerably. The temperature gradient predicted from the Fourier theory reduces significantly as compared to its counterpart predicted from electron kinetic theory. The difference in $\partial\phi/\partial x$ predicted from both theories is due to the temperature response of the material for a short laser heating pulse as indicated earlier. Moreover, the fast decay of $\partial\phi/\partial x$ before the point of minimum appears to have an almost similar trend for both theories. As the distance increases beyond the point of minimum, the trend of $\partial\phi/\partial x$ changes, which indicates that collisional process is as important as the conduction process due to phonon relaxation for the short heating pulse.

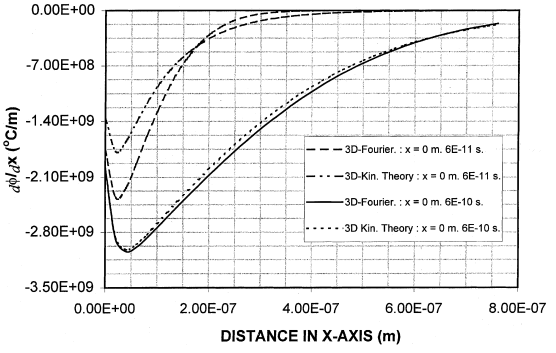

Fig. 7. $d\phi/dx$ predicted from the Fourier and kinetic theory along the y-axis for two pulse lengths and at different x-axis locations.

Fig. 8 shows the temperature profiles in the y-axis predicted from both theories at different x-axis locations for two pulse lengths. The temperature profiles predicted from both theories become almost similar. The small discrepancies are evident at the central region of the profiles. It should be noted that the peak temperature occurs at the center of the heated spot as marked in the figures. The discrepancies may be because of the effect of the power intensity in this region, i.e., the power intensity is maximum in this region. In this case, the radial heat transfer differs slightly for both models such that the Fourier theory results in slightly lower radial heat transfer as compared to electron kinetic theory, i.e., the temperature increases slightly in the central region of the heated spot in the Fourier heating case. This effect is also observed at different x-axis locations. On the other hand, the temperature profiles predicted from both

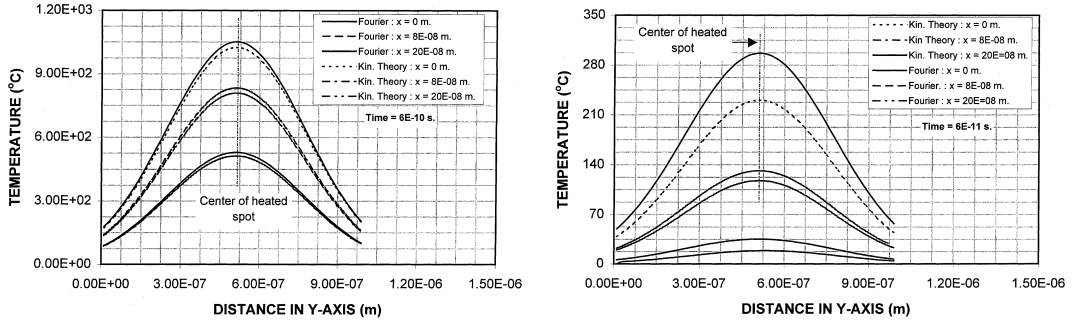

Fig. 8. Temperature profiles predicted from the Fourier and kinetic theory along the y-axis for two pulse lengths and at different x-axis locations.

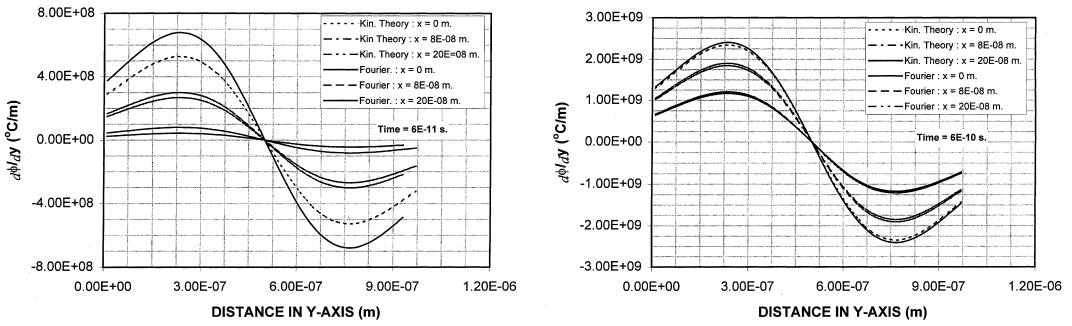

Fig. 9. $d\phi/dy$ predicted from the Fourier and kinetic theory along the y-axis for two pulse lengths and at different x-axis locations.

theories differ considerably for short pulse length. The difference between both temperature profiles is more pronounced at the workpiece surface where x-axis location is at the heated spot center ($x = 0$). This difference is because of the collisional process, which takes place substantially in the surface vicinity. Moreover, all the excess energy of the electrons cannot be transferred to lattice site atoms through the collisional process in the surface vicinity during a short heating time. Therefore, the excess energy of the electrons is transferred to lattice sites during further collisions in the region next to the surface vicinity as described earlier. As the location in the x-axis moves into the substrate, the difference between both predictions becomes small. This is again because of the collisional process. At a depth of 20×10^{-8} m, the temperature predicted from electron kinetic theory becomes higher than that corresponding to the Fourier theory. This indicates that the contribution of collisional process to the conduction energy transfer due to phonon relaxation is considerable, i.e., the energy transfer to lattice sites enhances with the collisional process taking place in this region.

Fig. 9 shows the variation of the temperature gradients in the y-axis ($\partial\phi/\partial y$) predicted from both theories with distance at different locations in the x-axis. The $\partial\phi/\partial y$ values predicted from both theories are almost identical for long pulse length. In general, $\partial\phi/\partial y$ attains the maximum value before it reduces to zero at the heated spot center. The energy balance among the absorbed energy, internal energy gain, and the conduction process occurs at the point of maximum, as explained earlier. As the x-axis location moves into the substrate, the slope of $\partial\phi/\partial y$ changes, but the point of maximum remains the same. In the case of short pulse length, $\partial\phi/\partial y$ distribution predicted from both theories differs considerably. This is because the energy exchange mechanisms take place in both theories. In this case, kinetic theory predicts relatively small slope of $\partial\phi/\partial y$ along the y-axis as compared to that predicted from the Fourier theory. The location of maximum $\partial\phi/\partial y$ in the y-axis remains the same for both theories.

4. Conclusion

In the present study, the temperature profiles predicted from electron kinetic theory approach and the Fourier heating model are compared for three- and one-dimensional heating cases. In general, temperature profiles for three- and one-dimensional heating cases are almost identical. This indicates that the three-dimensional heating approaches one-dimensional heating for a Gausssian power intensity profile. Moreover, the energy exchange mechanism taking place in the radial direction differs for both models during the short pulse heating. The Fourier heating model fails to predict correct temperature profiles at short heating duration. The electron kinetic theory predictions become similar to the findings of the two-equation model. The specific conclusions derived from the present study may be listed as follows:

1. The radial conduction in the central region of the heated spot is not considerable; in this case, the three-dimensional temperature predictions approach one-dimensional predictions.
2. Kinetic theory predicts lower temperatures in the surface vicinity of the substrate as compared to the Fourier theory results for the short pulse heating. The deviation of temperature profiles is because of different heating mechanisms considered in the analyses. In electron kinetic theory, not all the electron excess energy transfers to the lattice sites in the surface vicinity at short duration of the heating process. As the pulse length increases, and thus the heating time, the temperature predictions from both three- and one-dimensional models become identical.
3. The energy balance is attained at the point where $\partial\phi/\partial x$ becomes minimum in the surface vicinity. The location of the point of minimum for both theories is the same. At short pulse length, the change of the trend in $\partial\phi/\partial x$ occurs for both theories beyond the point of minimum. This reveals that the collisional process contributes to energy exchange mechanism as much as the phonon relaxation process due to lattice site temperature difference. The point of

minimum $\partial\phi/\partial x$ moves inside the substrate for the long length pulse heating.

4. The temperature profiles in the y-axis become almost the same for both theories at long length pulse, but considerable deviation in temperature profiles occurs at short pulse length heating processes. This indicates that the radial heat transfer differs considerably in the collisional process than in the classical conduction heating.
5. The energy balance is attained at a location in the y-axis, in which case $\partial\phi/\partial y$ is maximum. The location of the point of energy balance is independent of the x-axis locations.

Acknowledgements

The authors acknowledge the support of King Fahd University of Petroleum and Minerals, Dhahran, Saudi Arabia for this work.

References

[1] H.J. Zhang, Non-quasi-steady analysis of heat conduction from a moving heat source, ASME J. Heat Transfer 112 (1990) 777–779.
[2] B.S. Yilbas, Laser heating process and experimental validation, Int. J. Heat Mass Transfer 40 (5) (1997) 1131–1143.
[3] B.S. Yilbas, Analytical solution for time unsteady laser pulse heating of semi-infinite solid, Int. J. Mech. Sci. 39 (6) (1997) 671–682.
[4] B.S. Yilbas, The validity of Fourier theory of radiation heating of metals, Res. Mechanica 24 (1988) 377–382.
[5] B.S. Yilbas, S.Z. Shuja, Laser short pulse heating of surfaces, J. Phys. D, 1999, to be published.
[6] R.E. Harrington, Application of the theory of heat conduction to the absorption of blackbody radiation, J. Appl. Phys. 38 (1967) 3266–3271.
[7] S.I. Anisimov, B.L. Kapeliovich, T.L. Perel'man, Electron emission from metal surfaces exposed to ultra-short laser pulses, Sov. Phys. JETP 39 (1974) 375–377.
[8] G.L. Eesley, Picosecond laser studies of nonequilibrium electron heating in copper, in: D.H. Auston, K.B. Eisenthal (Eds.), Ultrafast Phenomena IV, 1984, pp.143–146.
[9] T.Q. Qiu, C.L. Tien, Short pulse laser heating on metals, Int. J. Heat Mass Transfer 35 (3) (1992) 719–726.
[10] T.Q. Qiu, C.L. Tien, Femtosecond laser heating of multi-layer metals – I. Analysis, Int. J. Heat Mass Transfer 37 (17) (1994) 2789–2797.
[11] A. Majumdar, Effect of interfacial roughness on phonon radiative heat conduction, ASME J. Heat Transfer 113 (1991) 797–805.
[12] D.Y. Tzou, A unified field approach for heat conduction from macro-to-micro-scales, ASME J. Heat Transfer 117 (1995) 8–16.
[13] L. Malinowski, A relaxation model for heat conduction and generation, J. Phys. D 26 (1993) 1176–1180.
[14] B.S. Yilbas, Heating of metals at a free surface by laser radiation an electron kinetic theory approach, Int. J. Eng. Sci. 24 (8) (1986) 1325–1334.
[15] B.S. Yilbas, A.Z. Sahin, An approach to convergency of kinetic theory to Fourier theory in relation to laser heating process, Jpn. J. Appl. Phys. 32 (Part 1) (1993) 5646–5651.
[16] G.D. Smith, Numerical Solution of Partial Differential Equations: Finite Difference Methods, third ed., Clarendon Press, Oxford, 1985.
[17] B.S. Yilbas, M. Sami, F. Al-Ferayedhi, Closed form and numerical solution to laser heating process, Inst. Mech. Engrs., Part C 212 (1998) 141–151.